Atomic Processes in Laser-Produced Tin Plasmas for the Efficient Emission of Extreme-Ultraviolet (EUV) Radiation

Akira SASAKI[1,2)]*, Atsushi SUNAHARA[3)], Katsunobu NISHIHARA[2)], Yu YAMAMOTO[2)], Nozomi TANAKA[2)], Shinsuke FUJIOKA[2)], Tomoyuki JOHZAKI[4)], Kentaro TOMITA[5)], Masashi YOSHIMURA[2)]

[1)] *QST, Kyoto 619-0215, Japan*
[2)] *University of Osaka, Osaka 565-0871, Japan*
[3)] *Purdue University, IN 47907, U.S.A.*
[4)] *Hiroshima University, Hiroshima 739-8511, Japan*
[5)] *Hokkaido University, Hokkaido 060-0808, Japan*

(Received 30 August 2025 / Accepted 30 September 2025)

The atomic processes in laser-produced tin plasmas for the extreme ultraviolet light sources are investigated. The level population of complex tin ions is calculated using the collisional-radiative (CR) model, and then spectral emissivity and opacity are calculated, taking the spectral structure of unresolved transition array into account. A rule-based method for developing a large-scale CR model is discussed, which enables the simulation of the emission spectrum using a relatively compact model. The effect of configuration interaction on the wavelength of the emission and broadening of the main peak at λ = 13.5 nm by the emission from multiply excited states is discussed.

Keywords: EUV source, multiple charged ion, collisional-radiative model, laser-pumped plasmas, plasma spectroscopy

DOI: 10.1585/pfr.21.2401001

1. Introduction

Extreme ultraviolet (EUV) lithography has been realized using laser-pumped plasma (LPP) sources [1]. More than 500 W of output power at the wavelength of λ = 13.5 nm into 2% bandwidth has been obtained with the 5% of conversion efficiency from CO_2 laser-pumped tin droplet using the pre-pulse technique [2]. The target material is dispersed by the irradiation of the pre-pulse laser, which is heated by the main-pulse laser when the material is expanded to an appropriate size to absorb the energy of the main-pulse laser. The irradiation by a second pre-pulse laser is useful for forming a uniform plasma with an appropriate density to improve the output power and efficiency [3].

Still higher power and efficiency of the EUV source are demanded for further miniaturization of semiconductor devices. For instance, the use of solid state lasers with the wavelength of λ = 2 μm laser has been proposed as a pumping source in place of the present CO_2 lasers [4]. Although the spectral purity from the solid state laser pumped plasma may be lower than CO_2 pumped plasma, it is expected to improve plug-in efficiency because of the higher electrical efficiency of the solid state lasers. We investigate the atomic processes in tin plasmas to provide the opacity table for the radiation hydrodynamics simulation for the optimization of the LPP EUV source. The optimum condition of the EUV source with respect to spectral purity of the plasma, coupling of the pumping laser to the target, and the effect of self-absorption will be investigated using the radiation hydrodynamics simulation.

The radiation transport has a significant effect on determining the temporal and spatial evolution of the plasmas. Therefore, the radiation hydrodynamics simulations are carried out using the opacity data, which is calculated taking into account the fact that the plasma state should be in non-local thermodynamic equilibrium (nLTE). The EUV spectrum is calculated taking into account the effect of optacity, which may cause a loss of light due to self-absorption. Therefore, the collisional-radiative (CR) model is developed, and the opacity and emissivity of the plasma for the steady-state population in collisional-radiative equilibrium (CRE) are calculated as a function of temperature and density without radiation, based on the investigation of atomic processes in tin plasmas [5].

2. Model

Tin ions have signature EUV emission. The emission arises from 4d–4f and 4p–4d atomic transitions of near 10 times

*Corresponding author's e-mail: sasaki.akira.ile@osaka-u.ac.jp
This article is based on the presentation at the Joint Conference of the 22nd International Conference on Atomic Processes in Plasmas (APiP 2025) and 1st NIFS Conference on Atomic and Molecular Processes in Plasmas.

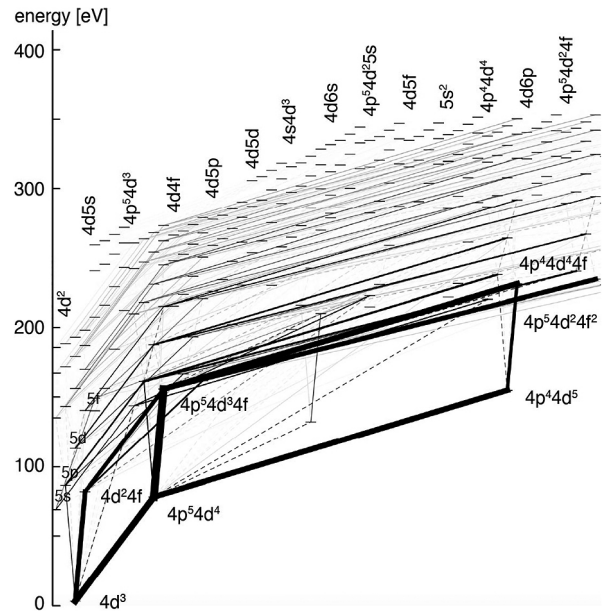

Fig. 1. Energy level diagram of Sn^{11+}. The line between levels shows the intensity of UTA by the line width that is calculated at an electron temperature of 35 eV, assuming LTE.

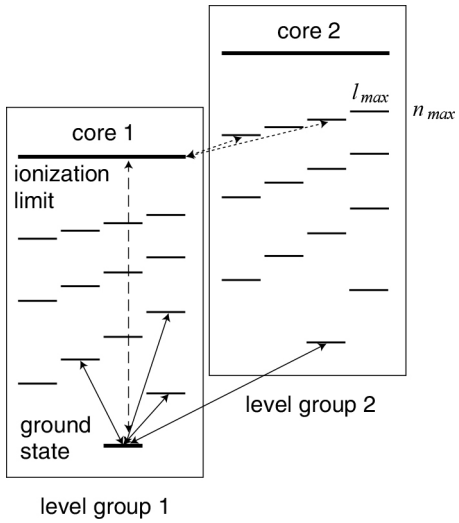

Fig. 2. Shematic diagram showing the process to develop the atomic model, showing that the model consists of a set of groups, which is a set of states with the same core and one excited electron.

ionized tin, showing a broad, strong peak at λ = 13.5 nm called an unresolved transition array (UTA) [6]. Figure 1 shows the energy level diagram of Sn^{11+}. Each atomic state consists of fine structure levels, and the transition between these states consists of a large number of fine structure transitions, so that the emission appears as UTA. Due to the effect of configuration interaction, 4d–4f and 4p–4d transitions appear as a single peak, and emission from a range of charged states in the plasma overlaps, resulting in efficient emission into a narrow bandwidth.

To calculate the spectral emissivity and opacity, we develop a CR model [7] of tin plasma based on the computational atomic data calculated using the HULLAC code [8]. As shown in Fig. 1, Sn^{11+} ion has the ground configuration of $4d^2$, and has the emission at λ = 13.5 nm through transitions from 4d4f and $4p^5$4d, one-electron excited states. However, the ion has a large number of possible multiply excited states. The ionization energy of the ground state of Sn^{11+} is 220 eV while the excitation energy of an electron from 4d to 4f orbit is 90 eV, so doubly and a part of triply excited state are below the ionization limit and can have a large population to emit a significant amount of EUV photons through 4d–4f and 4p–4d transitions, which should be included in the calculation of emissivity and opacity [9].

However, the fraction of atomic states that contribute to the emission to the number of possible states is relatively small. The model should be developed by extracting atomic states and transitions that have a significant effect on the spectrum and efficiency, while maintaining a tractable size of the model. We propose a method to develop the CR model, maintaining the completeness of the atomic model by including atomic states that have a significant contribution to the EUV emission.

Figure 2 shows the schematic diagram of the level structure used to determine the atomic model. The model is based on configuration-averaged (CA) atomic energy levels. To calculate the population, we need to include atomic states that have a small excitation energy and are likely to have a large population, and atomic processes such as excitation and ionization from/to these states. We define a group of atomic states that have the same core configuration with one excited electron. The atomic model is determined as the set of groups. The population of the atomic states in the groups is calculated by taking all possible excitation and ionization processes between the atomic states in the groups. To investigate the effect of multiply excited states, we include the atomic states group by group into the CR model. As shown in Fig. 2, this method allows one to include excitation processes between the states and ionization processes to the core state, which have large rates. For the excitation processes, the configuration between any pair of the two atomic states is investigated, and by finding the difference of only two orbits with the difference of orbital quantum number of corresponding electron is 1, then the dipole allowed transitions between states in different groups are also included. Furthermore, the autoionization from multiply excited states above the ionization threshold to available core states is included, so that dielectronic recombination processes are included.

We calculate energy levels, rates of radiative decay and autoionization using the HULLAC code. On the other hand, the rates of electron collisional excitation, collisional ionization, and radiative recombination are calculated using empirical formulas [10, 11]. The rates of inverse processes such as the electron collisional deexcitation and three-body recombination are calculated based on the detailed balance. The rate of dielectronic recombination is calculated by including autoionizing levels explicitly, and taking the electron capture, autoionization, and radiative decay for each level into account.

Table 1. List of a set of configurations that is used for the CR model of Sn^{9+} to Sn^{14+}. n is the index of level group. The range of principal and orbital quantum number of excited electron *nl* are $n \leq 8$ and $l \leq 3$, respectively.

n	Sn^{9+}	Sn^{10+}	Sn^{11+}	Sn^{12+}	Sn^{13+}	Sn^{14+}
1	$4s^24p^64d^4\,nl$	$4s^24p^64d^3\,nl$	$4s^24p^64d^2\,nl$	$4s^24p^64d\,nl$	$4s^24p^6\,nl$	$4s^24p^5\,nl$
2	$4s^24p^64d^35s\,nl$	$4s^24p^64d^25s\,nl$	$4s^24p^64d5s\,nl$	$4s^24p^54d^2\,nl$	$4s^24p^54d\,nl$	$4s4p^6\,nl$
3	$4s^24p^54d^5\,nl$	$4s^24p^54d^4\,nl$	$4s^24p^54d^3\,nl$	$4s^24p^65s\,nl$	$4s4p^64d\,nl$	$4s^24p^44d\,nl$
4	$4s^24p^64d^35p\,nl$	$4s^24p^64d^24f\,nl$	$4s^24p^64d4f\,nl$	$4s^24p^64f\,nl$	$4s^24p^44d^2\,nl$	$4s4p^54d\,nl$
5	$4s^24p^64d^34f\,nl$	$4s^24p^64d^25p\,nl$	$4s^24p^64d5p\,nl$	$4s^24p^65p\,nl$	$4s^24p^54f\,nl$	$4s^24p^34d^2\,nl$
6	$4s^24p^64d^35d\,nl$	$4s^24p^64d^25d\,nl$	$4s^24p^64d5d\,nl$	$4s^24p^65d\,nl$	$4s^24p^55s\,nl$	$4s^24p^44f\,nl$
7	$4s^24p^64d^36s\,nl$	$4s4p^64d^4\,nl$	$4s4p^64d^3\,nl$	$4s4p^64d^2\,nl$	$4s^24p^55p\,nl$	$4s^24p^45s\,nl$
8	$4s^24p^64d^25s^2\,nl$	$4s^24p^64d^26s\,nl$	$4s^24p^64d6s\,nl$	$4s^24p^44d^3\,nl$	$4s4p^54d^2\,nl$	$4s^24p^45p\,nl$
9	$4s^24p^64d^35f\,nl$	$4s^24p^64d5s^2\,nl$	$4s^24p^54d^25s\,nl$	$4s^24p^54d5s\,nl$	$4s^24p^55d\,nl$	$4p^64d\,nl$
10	$4s^24p^64d^36p\,nl$	$4s^24p^64d^25f\,nl$	$4s^24p^64d5f\,nl$	$4s^24p^54d4f\,nl$	$4s4p^64f\,nl$	$4s4p^44d^2\,nl$
11	$4s4p^64d^5\,nl$	$4s^24p^64d^26p\,nl$	$4s^24p^65s^2\,nl$	$4s^24p^66s\,nl$	$4s4p^65s\,nl$	$4s4p^54f\,nl$
12	$4s^24p^54d^45s\,nl$	$4s^24p^54d^35s\,nl$	$4s^24p^44d^4\,nl$	$4s^24p^65f\,nl$	$4s^24p^34d^3\,nl$	$4s^24p^45d\,nl$
13	$4s^24p^64d^24f5s\,nl$	$4s^24p^64d4f5s\,nl$	$4s^24p^64d6p\,nl$	$4s^24p^66p\,nl$	$4s^24p^44d4f\,nl$	$4s4p^55s\,nl$
14	$4s^24p^64d^25s5p\,nl$	$4s^24p^44d^5\,nl$	$4s^24p^54d^24f\,nl$	$4s^24p^54d5p\,nl$	$4s^24p^44d5s\,nl$	$4s^24p^24d^3\,nl$
15	$4s^24p^64d^36d\,nl$	$4s^24p^54d^34f\,nl$	$4s^24p^64f5s\,nl$	$4s^24p^66d\,nl$	$4s4p^65p\,nl$	$4s^24p^34d4f\,nl$
16	$4s^24p^54d^45p\,nl$	$4s^24p^64d^26d\,nl$	$4s^24p^64f^2\,nl$	$4s^24p^66f\,nl$	$4s^24p^55f\,nl$	$4s4p^55p\,nl$
17	$4s^24p^54d^44f\,nl$	$4s^24p^64d5s5p\,nl$	$4s^24p^54d^25p\,nl$	$4s^24p^54d5d\,nl$	$4s^24p^56s\,nl$	$4s^24p^34d5s\,nl$
18	$4s^24p^64d^36f\,nl$	$4s^24p^54d^35p\,nl$	$4s^24p^64d6d\,nl$	$4s4p^54d^3\,nl$	$4s^24p^56p\,nl$	$4s^24p^45f\,nl$
19	$4s^24p^44d^6\,nl$	$4s^24p^64d4f^2\,nl$	$4s^24p^65s5p\,nl$	$4s4p^64d5s\,nl$	$4s^24p^44d5p\,nl$	$4s^24p^46s\,nl$
20	$4s^24p^64d^24f5p\,nl$	$4s^24p^64d4f5p\,nl$	$4s^24p^64f5p\,nl$	$4s4p^64d4f\,nl$	$4p^64d^2\,nl$	$4p^54d^2\,nl$

The energy level structure of Sn^{11+} is determined firstly by choosing the core states of Sn^{12+} ion by the order of excitation energy, and secondly by adding one electron to any possible orbit, given the maximum principal and orbital quantum number *nl* of the electron. The number of the core states of Sn^{12+} corresponds to the number of groups of the states of Sn^{11+}. This procedure corresponds to taking the Cartesian product set of core configurations and an orbit of one electron, removing unphysical states. To calculate the spectral emissivity and opacity of tin plasmas for the EUV source, the model including Sn^{4+}–Sn^{32+} is produced by repeating the production of atomic states and calculation of their energy using the HULLAC code, and descending the ion charge recursively. Using the present method, we can develop the atomic model in a reproducible way, and the size of the model can be controlled according to the number of groups and principal and orbital quantum numbers of the excited electron.

Table 1 shows the list of configurations of Sn^{9+} to Sn^{14+}, which is used to calculate the spectral emissivity and opacity, including 20 groups of excited states. We solve the set of rate equations to obtain the population and ion fraction. Typically, calculations are carried out with a total number of states of 5,000 and using the Monte-Carlo method [12]. Subsequently, applying the profile of each UTA to calculate the spectral emissivity and opacity. The profiles are obtained by the detailed line-by-line calculations using the HULLAC code, taking the effect of configuration interaction into account. The UTA sometimes consists of more than 1,000 fine structure transitions. We defined the profile of each UTA from the distribution of lines, with the energy mesh of the spectrum of 0.2 eV. Furthermore, as the calculated wavelength of the UTA that corresponds to 4d–4f and 4p–4d transitions differs from experiment, the calculated wavelength is shifted to fit the experimental spectrum for each charge state [13].

3. Results

Figure 3 shows the spectral emissivity of tin plasma, calculated at the temperature and ion density of the plasma of 31 eV and 1.0×10^{19} cm^{-3}. The results of the calculation for the number of groups of excited states of 1, 5, and 20 are shown. Only with 1 group, one electron excited states from the ground state ($4d^2$), the width of the UTA at λ = 13.5 nm is significantly narrower, and the emissivity is underestimated. With 5 groups of excited states, emission from multiply excited states is included to show the broad structure in the

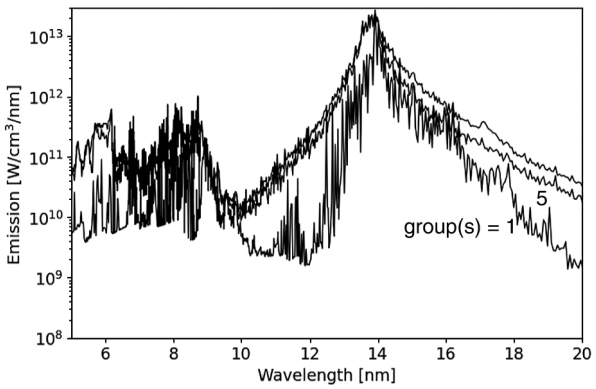

Fig. 3. Spectral emissivity of tin plasmas calculated at the electron temperature and density of 31 eV and 1.0×10^{19} cm^{-3}. Results calculated with 1, 5, and 20 groups of excited states.

shorter and longer wavelength regions of the main peak. Due to the large statistical weight, the 4d–4f and 4p–4d transitions from multiply excited states have comparable intensity with those from singly excited states, that appears near λ = 13.5 nm but have a broader spectral width. The emissivity of the longer wavelength region further increases as the number of groups of excited states is increased to 20, but the difference from those with 5 groups of excited states is small, suggesting the convergence of emissivity with respect to the effect of multiply excited states.

An increase of the intensity of UTA is also seen in the wavelength region λ = 6–10 nm, which are attributed to 4p–5s, 4d–6p, and 4d–5p transitions.

4. Discussion

We develop a CR model of tin to calculate the emissivity and opacity of tin plasmas for the EUV source. We propose a rule-based method, by determining the set of atomic states that have the same core configuration and one excited electron, to capture the significant atomic states and atomic processes in the plasma. The atomic model is produced automatically using a few parameters, which determine the size of the model. After a convergence analysis of results, population as well as spectral emissivity and opacity can be calculated with a relatively small size of the model [14].

The effect of emission from multiply-excited tin ions are shown. It is found that the emission from multiply-excited states contributes not only to the main 4d–4f and 4p–4d UTA but to 4p–5s, 4d–5p, and 4d–6p UTAs.

The present method can be applicable to model other atomic elements, to investigate the properties of rare-earth elements such as Gd and Tb, and heavier elements as Bi, to optimize the power and efficiency of the future plasma sources in the wavelengths of λ = 4–6 μm.

Validation of the results had been carried out from the validation of the atomic data to the calculation method. However, difficulty arises from the large volume of atomic data, such as energy levels and cross sections, which have been difficult to validate independently. Therefore, as an alternative method of validation, comparisons between different codes have been carried out in nLTE kinetics workshop to validate the CR model [15]. Furthermore, atomic processes and emission spectrum, specific to the EUV source are validated in EUVL source workshop [16]. Reliability of the model should be improved through comparisons between calculation and experiment, especially those recent joint measurements of the density and temperature profiles of the plasma and the EUV emission spectrum [17].

Acknowledgement

The author AS acknowledges a useful discussion with I. Murakami and D. Kato at the National Institute for Fusion Science, and support from Dr. M. Ishino, Dr. R. Itakura, Dr. M. Kando, and Dr. T. Kawachi of the National Institutes for Quantum Science and Technology. This work was supported by JST K Program Grant Number JPMJKP24M1. This work was also supported JSPS grants 21H04460, and 23H01147.

[1] *EUV Lithography*, V. Bakshi (SPIE press, 2018).
[2] H. Mizoguchi *et al.*, Proc. of SPIE **10143**, 10143J-1 (2017).
[3] Q. Zhu *et al.*, Proc. of SPIE **13424**, 13240Y-1 (2025).
[4] R. Schupp *et al.*, J. Phys. D **54**, 365103 (2021).
[5] K. Nishihara *et al.*, Phys. Plasmas **15**, 056708 (2008).
[6] W. Svendsen *et al.*, Phys. Rev. A **50**, 3710 (1994).
[7] *Modern Methods in Collisional-Radiative Modeling of Plasmas*, Yu. Ralchenko (Springer, 2016).
[8] A. Bar-Shalom *et al.*, J. Quant. Spectrosc. Radiat. Transfer **71**, 169 (2001).
[9] F. Torretti *et al.*, Nature. Commun. **11**, 2334 (2020).
[10] W. Lotz, Z. Phys. **216**, 241 (1968).
[11] R. Mewe, Astron. Astrophys. **216**, 215 (1972).
[12] A. Sasaki *et al.*, HEDP **32**, 1 (2019).
[13] H. Ohashi *et al.*, J. Phys. B: At. Mol. Opt. Phys. **43**, 065204 (2010).
[14] A. Sasaki, Appl. Phys. Lett. **124**, 064104 (2024).
[15] R. Piron *et al.*, HEDP **23**, 38 (2017).
[16] Proceedings of the 2023 EUVL source workshop, V. Bakshi *et al.*, https://www.euvlitho.com/2023/2023 (2023).
[17] Y. Pan *et al.*, Appl. Phys. Lett. **123**, 204103 (2023).